

# Two-Photon Microscopy and Fluorescence Lifetime Imaging of Retinal Pigment Epithelial Cells Under Oxidative Stress

Yoko Miura,<sup>1,2</sup> Gereon Huettmann,<sup>1</sup> Regina Orzekowsky-Schroeder,<sup>1</sup> Philipp Steven,<sup>3</sup> Márta Szaszák,<sup>4</sup> Norbert Koop,<sup>1</sup> and Ralf Brinkmann<sup>1</sup>

<sup>1</sup>Institute of Biomedical Optics, University of Lübeck, Lübeck, Germany

<sup>2</sup>Department of Ophthalmology, University of Lübeck, Lübeck, Germany

<sup>3</sup>Department of Ophthalmology, University of Cologne, Cologne, Germany

<sup>4</sup>Institute of Medical Microbiology and Hygiene, University of Lübeck, Lübeck, Germany

Correspondence: Yoko Miura, Institute of Biomedical Optics, University of Lübeck, Lübeck, Germany, Peter-Monnik-Weg 4, 23562 Lübeck, Germany; Miura@bmo.uni-luebeck.de.

Submitted: February 3, 2013

Accepted: March 26, 2013

Citation: Miura Y, Huettmann G, Orzekowsky-Schroeder R, et al. Two-photon microscopy and fluorescence lifetime imaging of retinal pigment epithelial cells under oxidative stress. *Invest Ophthalmol Vis Sci*. 2013;54:3366-3377. DOI:10.1167/iov.13-11808

**PURPOSE.** The aim of this study was to investigate the autofluorescence (AF) of the RPE with two-photon microscopy (TPM) and fluorescence lifetime imaging (FLIM) under normal and oxidative stress conditions.

**METHODS.** Porcine RPE-choroid explants were used for investigation. The RPE-choroid tissue was preserved in a perfusion organ culture system. Oxidative stress was induced by laser photocoagulation with frequency-doubled Nd:YAG laser (532 nm) and by exposure to different concentrations (0, 1, 10 mM) of ferrous sulfate (FeSO<sub>4</sub>) for 1 hour. At indicated time points after exposure, the tissue was examined with TPM and FLIM. Intracellular reactive oxygen species around the photocoagulation lesion were detected with chloromethyl-2'-7'-dichlorofluorescein diacetate (CM-H2DCFDA). Melanosomes were isolated from RPE cells and their fluorescence properties were investigated under normal and oxidized conditions.

**RESULTS.** Under normal conditions, AF in RPE cells with TPM is mostly originated from melanosomes, which has a very short fluorescence lifetime (FLT; mean = 117 ps). Under oxidative stress induced by laser irradiation and FeSO<sub>4</sub> exposure, bright granular AF appears inside and around RPE cells, whose FLT is significantly longer (mean = 1388 ps) than the FLT of the melanosome-AF. Excitation and emission peaks are found at 710 to 750 nm and 450 to 500 nm, respectively. Oxidative stress increases the fluorescence intensity of the melanosomes but does not change their FLT.

**CONCLUSIONS.** TPM reveals acute oxidative stress-induced bright AF granules inside and around RPE cells which can be clearly discriminated from melanosomes by FLIM. TPM combined with FLIM is a useful tool of live-cell analysis to investigate functional alterations of the RPE.

**Keywords:** retinal pigment epithelium, laser photocoagulation, two photon microscopy, fluorescence lifetime imaging, oxidative stress

Due to its deep tissue penetration and limited photochemical damage, two-photon microscopy (TPM) has been applied in different fields of tissue research.<sup>1-3</sup> Besides analysis of artificial fluorophores, this technique enables also the detection of two-photon-excited autofluorescence (AF) signals in living animals.<sup>4-6</sup> The principle of a two-photon microscope is characterized as simultaneous absorption of two photons in order to obtain the same fluorescence as in one photon excitation with half the wavelength (Fig. 1A). The simultaneous two-photon absorption is possible only at the focal plane, so that the fluorophores outside of the focal plane are not excited (Fig. 1B). Therefore, the pinhole as used in the confocal laser scanning microscope is not required in order to obtain a sharp image from one plane in a tissue volume. These properties of TPM enable three-dimensional analysis of deeper tissue with minimal loss of fluorescence and reduced phototoxicity.

AF is one of the important tissue properties that indicate cellular metabolic states or functional alterations. AF in living tissue may derive from different fluorophores: NAD(P)H,<sup>7</sup>

flavins,<sup>8</sup> porphyrin,<sup>9</sup> lipofuscin,<sup>10</sup> collagen,<sup>11</sup> elastin,<sup>12</sup> and other sources. In clinical ophthalmology, measurement of fundus AF derived from lipofuscin in RPE cells is practically utilized as a tool to assume functional alterations of the RPE and the prediction of disease prognosis.<sup>13,14</sup> However, recent studies suggest that there might be many other AF sources that are responsible for the change of fundus AF than lipofuscin.<sup>15-18</sup>

Each fluorophore has its own characteristic fluorescence property, as excitation/emission spectrum or fluorescence lifetime (FLT). FLT is determined as the time when the energy state of the fluorophore drops down to  $1/e$  (approximately 36%) from the initial excited energy value. FLT is an intrinsic character of each fluorescent molecule and is independent of fluorescence intensity. Therefore, fluorescence lifetime imaging (FLIM) enables discriminating different fluorophores. Moreover, FLT is used as a biomarker of the local environment of the fluorophore. Changes of the FLT reflect the alterations of the biological environment of the fluorescent molecule, such as temperature, pH, redox state, or the protein-binding state.<sup>19-22</sup>

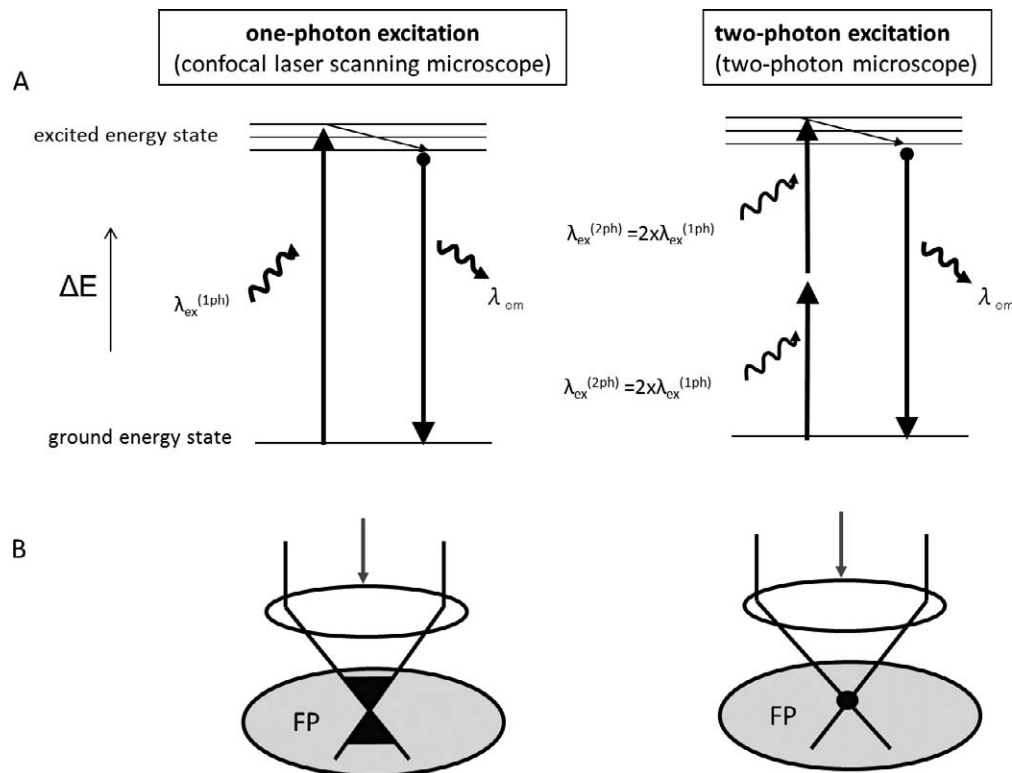


**FIGURE 1.** Schematic drawing for the comparison between one-photon excitation and two-photon excitation. **(A)** Energy level diagram. *Left:* In one-photon excitation, one photon of the light ( $\lambda_{\text{ex}}^{(1\text{ph})}$ ) with appropriate energy ( $\Delta E$ ) excites the targeted molecule and raises its energy state from ground to excited level. The excited molecule can relax to its lowest vibrational level in the excited state, from where it can return to the ground state by emitting a photon. *Right:* In two-photon excitation, two photons of twice the wavelength ( $\lambda_{\text{ex}}^{(2\text{ph})} = 2 \times \lambda_{\text{ex}}^{(1\text{ph})}$ ), and half the energy ( $1/2 \Delta E$ ) are absorbed simultaneously to excite the molecule to reach the excited energy level. **(B)** *Left:* In one-photon microscope, all dye molecules along the beam-path outside the focal point (FP) are also excited and thus out-of-focus light has to be eliminated using a pinhole. *Right:* In two-photon microscope, only dye molecules within the FP are excited, thus there is no need for a pinhole.

There are basic science evidences suggesting that decrease in RPE cell function is significantly related to the pathogenesis of chorioretinal disorders, such as AMD.<sup>23–25</sup> In particular, oxidative stress, for example induced by iron, is suggested as one of the potential factors in AMD.<sup>26</sup> Although new treatments for the advanced form of wet-type AMD, such as VEGF antagonists, have significantly improved the clinical results in the last decades,<sup>27,28</sup> disease progression still cannot be stopped in many cases. Therefore, improving early disease detection as well as prophylactic treatments is desired today. Noninvasive and sensitive detection of the functional alteration of RPE cell might be a useful tool for early diagnosis. We hypothesized that AF and FLT can indicate functional alterations of RPE cells that are induced by oxidative stress. Therefore, in this study, we investigated RPE-AF with TPM and FLIM at the cellular level under physiological and oxidative stress conditions.

## MATERIALS AND METHODS

### RPE-Choroid Tissue

Porcine RPE-choroid tissue explants were prepared and cultured as previously described.<sup>29</sup> The freshly enucleated porcine eyes were preserved in a cool and dark condition until preparation. The anterior part of the eye and the vitreous were removed, and the retina-RPE-choroid sheets were separated from the sclera using forceps and scissors. The retina was gently removed, leaving the RPE untouched. Prepared tissue was fixed between the lower and upper part of the tissue

carrier (Minusheets; Minucells and Minutissue, Bad Abbach, Germany), excess tissue was removed and the ring was placed in a culture container (Minucells and Minutissue). The chamber was placed on a heating plate (37°C). The culture medium was a mixture of equal amount of Dulbecco's modified Eagle's medium (DMEM; PAA, Cölbe, Germany) and Ham's F12 medium (PAA), which was supplemented with penicillin/streptomycin (1%), L-glutamine, 4-(2-hydroxyethyl)-1-piperazineethanesulfonic acid (HEPES; 25 mM); sodium pyruvate (110 mg/L); and 10% porcine serum (PAA). The container's volume is approximately 5 mL and the velocity of medium flow is 1.5 mL/h. The medium enters the container at its front end, passes between the tissue carriers, and leaves the container at the rear side.

### Two-Photon Microscopy

The RPE-choroid tissue explants were investigated using multiphoton tomography (DermaInspect; JenLab GmbH, Neuenbürg, Germany), which consists of 80-MHz titanium:sapphire laser (MaiTai; Spectra Physics, Darmstadt, Germany) with a tuning range of 710 to 920 nm. For the investigation, the tissue was placed with the RPE side up in the culture dish with culture medium and kept at 37°C. A  $\times 20$  water immersion objective with numerical aperture (NA) 1.0 and 2-mm working distance was used (W Plan-Apochromat  $\times 20$ , 1.0; Carl Zeiss Meditec, Göttingen, Germany). RPE-AF was detected by a photomultiplier module (H7732; Hamamatsu Photonics Deutschland GmbH, Herrsching, Germany), which detects the fluorescence bandwidth from 380 to 680 nm. Excitation spectral analysis was performed by measuring fluorescence

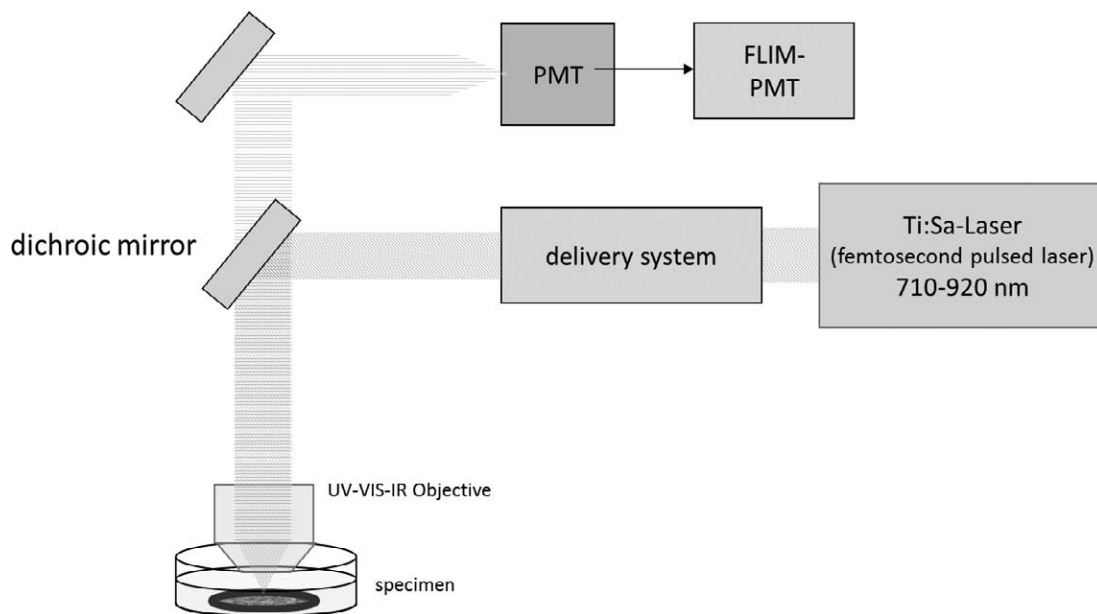


**FIGURE 2.** Schematic drawing of the experimental setup of TPM and FLIM. The tissue was placed with the RPE side up in the culture dish with culture medium and kept at 37°C. The objective is a  $\times 20$  water immersion objective with NA 1.0 and a 2-mm working distance. The RPE-AF was detected by a standard photomultiplier module (PMT), which detects the fluorescence bandwidth from 380 to 680 nm. For the FLT measurement, a fast PMT module for FLIM was used to generate a start signal and a stop signal by a next reference pulse from the light source.

intensity of the region of interest at each wavelength (every 10 nm from 710 to 900 nm) followed by normalization to irradiation power and pulse length for each wavelength.<sup>30</sup> For comparison, spectra were normalized to the intensity at 710 nm. For the emission spectral imaging, we inserted a four-channel spectral detector (channel 1: 380–450 nm, channel 2: 450–500 nm, channel 3: 500–580 nm, channel 4: 580–680 nm; JenLab GmbH, Jena, Germany) into the fluorescence path consisting of four photomultiplier tubes (Hamamatsu R1294A and R1295A, Hamamatsu Photonics Deutschland GmbH) and a

set of dichroic filters as described previously.<sup>30</sup> For the spatial investigation,  $z$ -series analysis was performed followed by the image reconstruction with commercial imaging software (Imaris; Bitplane Inc., South Windsor, CT).

### Fluorescence Lifetime Imaging (FLIM)

FLIM was performed using time-correlated single photon counting (TCSPC) method.<sup>31</sup> Start signals for counting were generated from a fast photomultiplier module (PMH-100-0; Becker & Hickl, Berlin, Germany) that detects the fluorescence

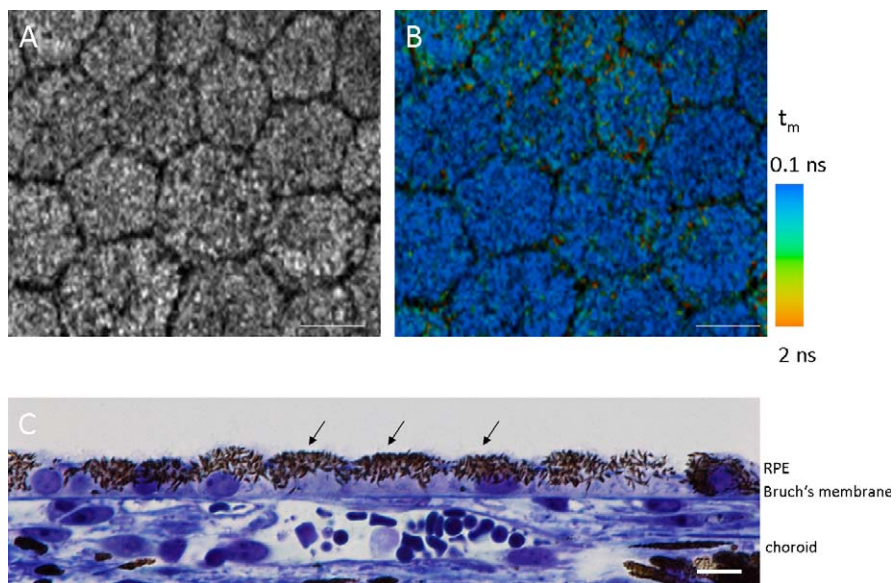


**FIGURE 3.** TPM-AF and FLIM image of ex vivo RPE under normal conditions. (A) TPM-AF of RPE with 750-nm excitation from apical side. Granular AF signals inside cells are observed. (B) FLIM image of the AF shown in (A). The most AF inside the RPE have a short FLT (blue colored), which is characteristic for melanosome-AF  $t_m$ : mean FLT. (C) Histological section of the explant shows a number of melanosomes (arrows) located at the cells' apical side. Scale bar: 10  $\mu$ m (A–C).

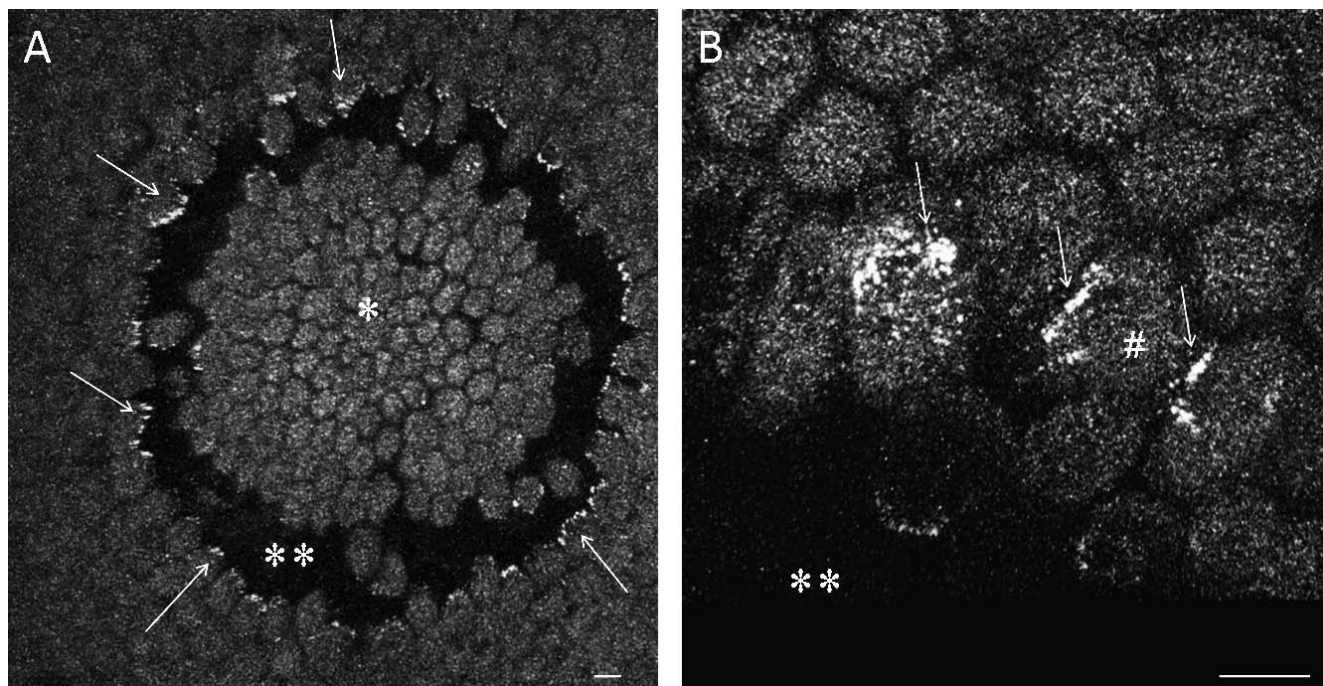


**FIGURE 4.** TPM images 24 hours after thermal laser irradiation on the RPE. **(A)** TPM-AF of a whole coagulation spot at 750-nm excitation. Bright AF signals appeared around the coagulated area (*arrows*). The cells in the center (\*) are the coagulated RPE cells and the black area (\*\*) is a RPE crack formed by the shrinkage and the shift of the coagulated RPE cells. **(B)** A magnified image of **(A)**. The induced AF (*arrows*) are much brighter than the melanosome-AF (#) and can be observed inside and around the cells. *Scale bar*: 10  $\mu\text{m}$  (**A**, **B**).

photons emitted by the tissue. The stop signal was provided by the next reference pulse from the light source. The timing lack between start and stop signals was measured by a single-photon counting board (SPC 830; Becker & Hickl). All the photons that arrive at the detector (H5773; Hamamatsu Photonics Deutschland GmbH) in a different time bin are counted. The measured decay curve was fitted to a single or multiexponential curve, which was convoluted with the instrumental response function. Due to the instrumental response function, the shortest resolvable FLT component was approximately 90 to 100 ps. The mean fluorescence lifetime was calculated for each pixel and displayed in color-coded images (SPCImage 2.6; Becker & Hickl). Fluorescence intensity is a sum of each discrete exponential, described as,

$$I(t) = \sum \alpha_i \exp\left(-\frac{t}{\tau_i}\right). \quad (1)$$

$I(t)$  stands for the fluorescence intensity at the time point  $t$ , and  $\alpha_i$  and  $\tau_i$  are the amplitude and the fluorescence decay time of  $i$ th component, respectively.

The mean lifetime ( $\tau$ ) for the multiexponential decays of fluorescence is obtained through,

$$\tau = \frac{\sum \alpha_i \tau_i^2}{\sum \alpha_i \tau_i}. \quad (2)$$

The schematic drawing of experimental setup of TPM and FLIM is shown in Figure 2.

### Laser Irradiation

RPE cells were irradiated by photocoagulation laser, which is considered to induce strong oxidative stress responses in the surrounding area of coagulation. For laser irradiation, the RPE

tissue explants were placed in a cell culture dish with 2.5 mL PBS and irradiation started immediately at a wavelength of  $\lambda = 532$  nm with a double-frequency YAG laser. The laser was coupled to a slit lamp, at which a mirror was placed in the beam path. This ensures vertical irradiation of the tissue that is placed horizontally on the stage. The tissue was irradiated with the following conditions: spot diameter 300  $\mu\text{m}$ , irradiation time 100 ms, and laser power 50 mW and 80 mW. After laser irradiation, the tissue was placed back to the perfusion culture container and maintained until the indicated time points of investigation with TPM and FLIM.

### Detection of Reactive Oxygen Species Around the Laser Spots

Intracellular reactive oxygen species (ROS) were detected using chloromethyl-2',7'-dichlorofluorescein diacetate (CM-H2DCFDA)-AM (Life Technologies GmbH, Darmstadt, Germany). CM-H2DCFDA-AM is nonfluorescent when chemically reduced. Intracellular esterases convert it to CM-H2DCFDA followed by the conversion to fluorescent DCF by intracellular ROS, which can be detected with excitation 485 nm/emission 530 nm (one-photon excitation). Under two-photon excitation, the strongest fluorescence was detected when excited with 750 nm. Three hours after laser irradiation, tissue AF of the RPE was investigated with TPM. After initial AF imaging, CM-H2DCFDA-AM (10  $\mu\text{M}$ ) was added carefully under dark conditions into the culture medium. After waiting for 15 minutes, the DCF fluorescence was imaged with 750 nm excitation. Uniformly distributed DCF fluorescence is to be detected in the cytoplasm if ROS was formed in RPE cell. During investigation, the culture dish was kept in 37°C. Medium-pH was stabilized by adding HEPES in culture medium.

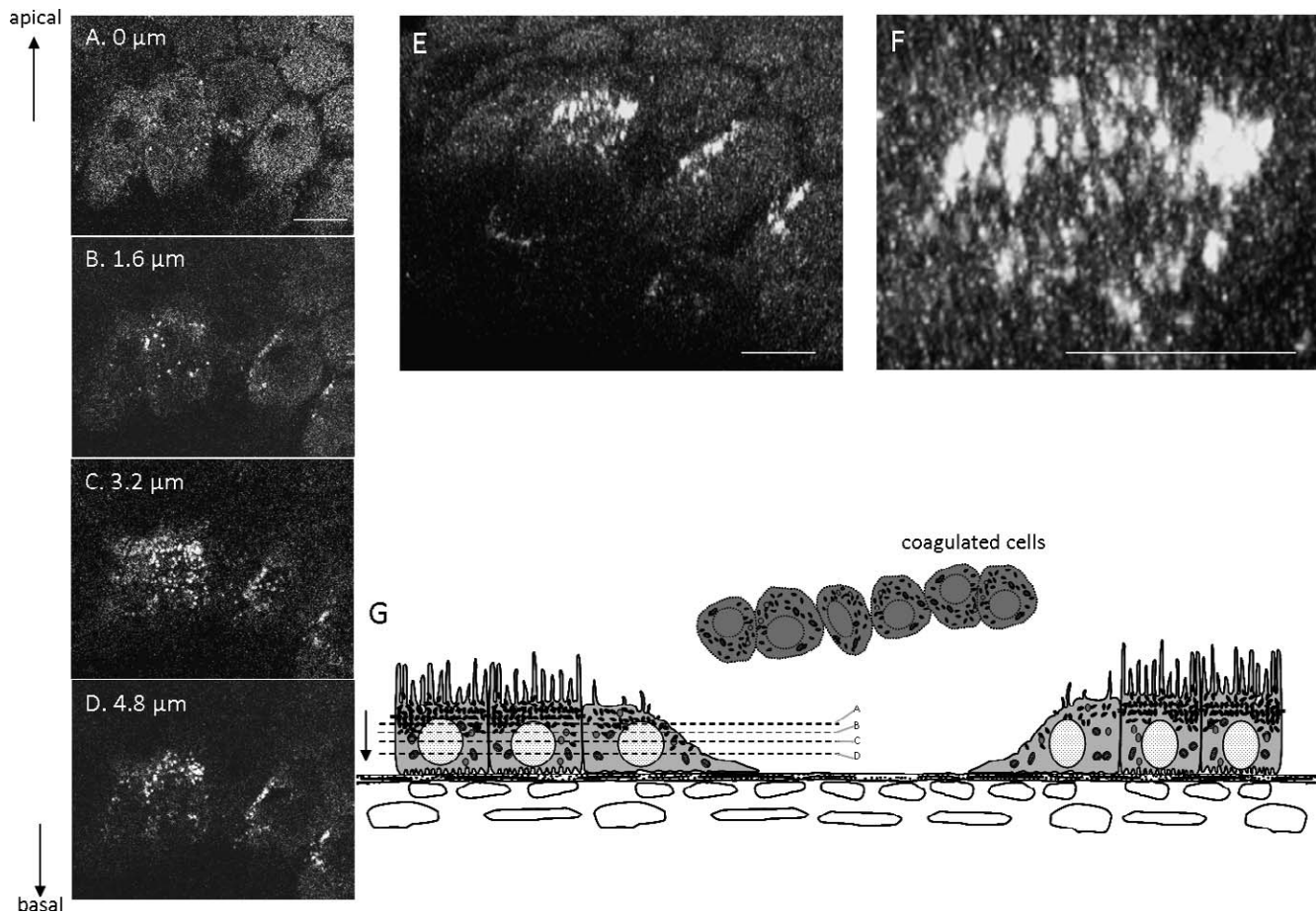


**FIGURE 5.** Z-series and 3D reconstruction of bright AF spots in RPE cells around photocoagulation. (A–D) Z-series (apical to basal) of TPM-AF of the lesion shown in Figure 4B. The bright AF signals are distributed from apical to basal side of the RPE cell. (E, F) 3D reconstruction by stacking image analysis with Imaris software. The form of the bright AF varies from round to slightly cylindrical. (G) A schematic drawing of the lesion around the photocoagulation spot 24 hours after irradiation. The slices for the z-series shown in (A–D) are presented schematically. Scale bar: 10  $\mu\text{m}$  (A–F).

### Induction of Lipid Peroxidation With $\text{FeSO}_4$

Iron was used to induce lipid peroxidation of the tissue as described previously.<sup>32–35</sup> In order to examine if the nonenzymatic lipid peroxidation leads to the alteration of AF in the RPE cells, different concentration (0, 1, 10 mM) of ferrous sulfate heptahydrate ( $\text{FeSO}_4 \cdot 7\text{H}_2\text{O}$ ; Sigma-Aldrich, St. Louis, MO) was added to the tissue culture medium and incubated for 1 hour. After that, the medium was completely replaced by the normal culture medium and then tissue AF was investigated with TPM and FLIM.

### Isolation of Melanosomes From RPE Cell

Melanosomes from porcine RPE cells were isolated as previously described.<sup>36</sup> Briefly, after removing the neural retina, RPE cells were gently brushed off from Bruch's membrane using a camel hair brush and collected in PBS. The cells were sonicated and the cellular debris was removed by centrifugation at 60g for 7 minutes. The pigment granules could be sedimented by centrifuging the resultant from last low-speed centrifugation with 6000g for 10 minutes. The sedimented pigment granules were suspended in 0.3 M sucrose and layered onto a sucrose gradient solution (2.0, 1.8, 1.6, 1.5, 1.4, 1.2, 1.0 M) and centrifuged with an ultracentrifuge at 103,000g for 1 hour. The melanosomes formed a pellet. The pellet was washed four times with PBS to remove the sucrose.

### Oxidation of Isolated Melanosomes

RPE-melanosomes isolated as described above were kept in culture medium. The fluorescence characteristics (fluorescence spectrums with TPM and FLIM) of RPE-melanosomes were analyzed under normal condition (no stimulation, in culture medium, at 37°C) and oxidized condition, which was induced by the exposure to  $\text{H}_2\text{O}_2$  (1 mM) for 1 hour.

### Histological Analysis

Some RPE-choroid tissues were prepared for the histological analysis in order to confirm good morphological polarities of the tissue used in the study and to refer to the TPM results. The tissue was fixed with Monti-Graziadei solution (2% glutaraldehyde and 0.6% paraformaldehyde), and after primary fixation, the tissue was washed and subjected to secondary fixation by 1% osmium tetroxide. After dehydration in rinsing alcohol series (30%–100%) and embedding in araldite, the tissue was embedded in epoxy resin. A semi-thin section (600-nm thickness) was stained with toluidine blue and examined with light microscopy.

### Statistical Analysis

All experiments were conducted in triplicate and the results are expressed as the mean  $\pm$  SD. Statistical analyses were

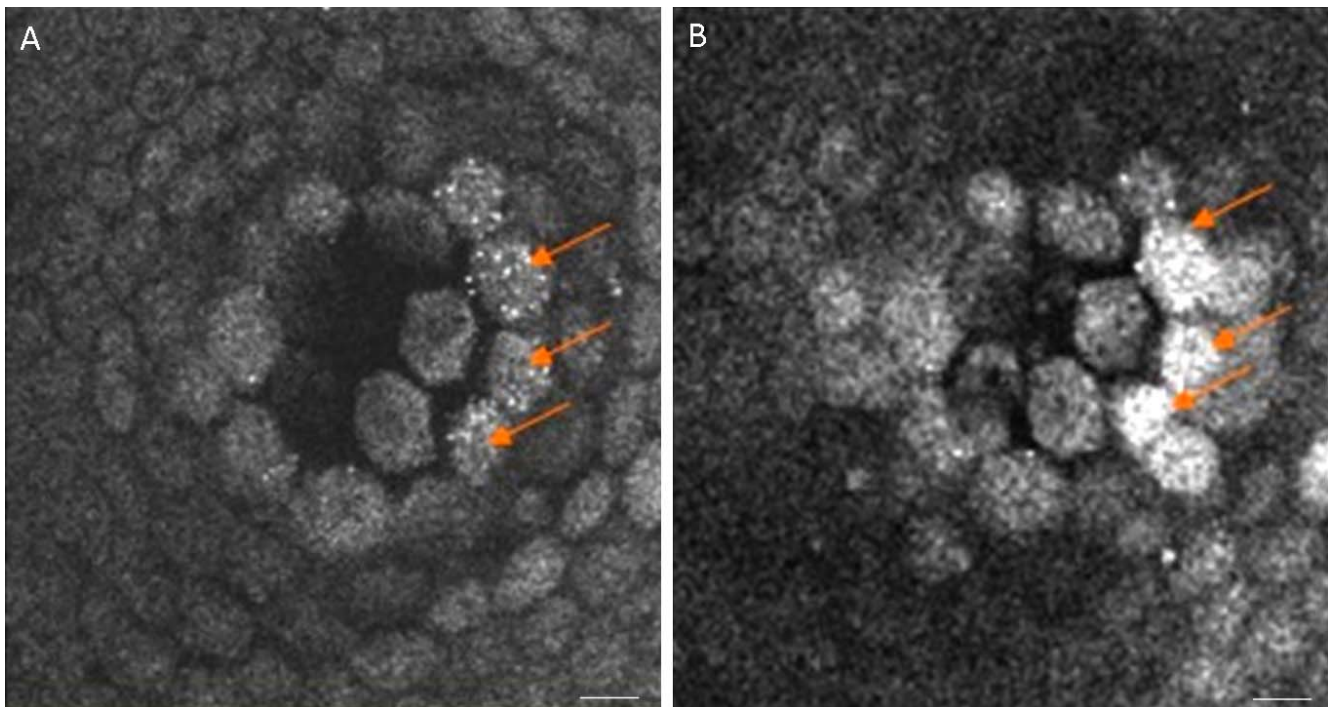


**FIGURE 6.** Detection of ROS in RPE cells after photocoagulation. (A) TPM-AF ( $\lambda_{\text{ex}} = 750$  nm) of RPE cells irradiated with the power of 50 mW for 0.1 s. Beam diameter was 300  $\mu\text{m}$ . In some RPE cells around the coagulation center, bright AF spots appear (arrows). (B) Fluorescence after application of the ROS indicator H2DCFDA-AM ( $\lambda_{\text{ex}} = 750$  nm). H2DCFDA-AM turns fluorescent CM-H2DCFDA in the existence of intracellular ROS. The strong fluorescence of CM-H2DCFDA is observed at the rim of the coagulation site, which correlates well with the appearance of the bright AF spots observed in (A). Scale bar: 10  $\mu\text{m}$  (A, B).

performed with Student's *t*-test, and the two-sided *P* value less than 0.05 was determined as significant.

## RESULTS

### AF of Porcine RPE Cells With TPM

Figure 3A shows the AF image of porcine RPE in culture medium under normal conditions at 37°C observed by TPM at an excitation wavelength of 750 nm. Fluorescence is detected from 360 to 680 nm. Granular AF is visible inside the RPE cells. Figure 3B is the FLIM image of the AF shown in Figure 3A. The FLT is presented as a pseudocolor image, where a blue color indicates a short FLT ( $\approx 0.1$  ns) and an orange color a long FLT ( $\approx 3.0$  ns). As seen in Figure 3B, most of the AF inside the RPE cells have a very short FLT around 100 ps, shown in blue. This short-lifetime granular fluorescence is considered to be caused by melanosomes, which are distributed at the apical side of RPE cells. Melanin has a bright two-photon AF, which has short FLT around 100 ps.<sup>37,38</sup> The apical occupation of the melanosomes in porcine RPE cells is confirmed in the histological study of a semi-thin section shown in Figure 3C.

### AF Induced by Photocoagulation

From a few hours after photocoagulation, bright granular AF spots are observed inside and around some RPE cells around the photocoagulation spot (Fig. 4). These bright AFs are observed from 1 hour to 72 hours after photocoagulation, with the highest number of granules observed 24 hours after laser irradiation and afterward, a gradual disappearing over time.

Stacking image analysis (*z*-series) reveals that many of the laser-induced bright fluorescent granules are located inside the cell (Figs. 5A–D, 5G) and their size is variant (diameter 1–2  $\mu\text{m}$ ,

length 2–4  $\mu\text{m}$ ) and their shape is from round to cylindrical (Figs. 5E, 5F).

### Increased ROS Formation Around Photocoagulation Sites

Increased ROS is detected in the RPE cells around the site of photocoagulated lesions (Fig. 6). Prominently strong ROS signals are observed inside the RPE cells (Fig. 6B), in which bright granular AF spots appear (Fig. 6A). This result suggests that the appearance of bright AF spots around the photocoagulation sites is related to the intracellular ROS formation induced by thermal exposure.

### Increased AF Induced by Iron

Influence of iron-induced oxidative stress on RPE-AF was investigated using  $\text{FeSO}_4$  treatment. One-hour exposure to  $\text{FeSO}_4$  induces bright granular AF signals inside and around RPE cells in a dose-dependent manner (Fig. 7), where 10 mM  $\text{FeSO}_4$ -exposed RPE cells appear to be morphologically strongly damaged. The size and form of these AF spots are similar to the granular AF spots detected around photocoagulation sites.

### Fluorescence Properties of Laser-/Iron-Induced AF Signals

**Excitation Spectrum.** Figure 8A shows the excitation spectrum of laser- or iron-induced bright AF spots and the melanosome-AF, which was normalized to excitation power and pulse length. For comparison, spectra were normalized to the intensity at 710 nm. While melanosome-AF intensity reduces largely at the excitation wavelength around 740 nm,

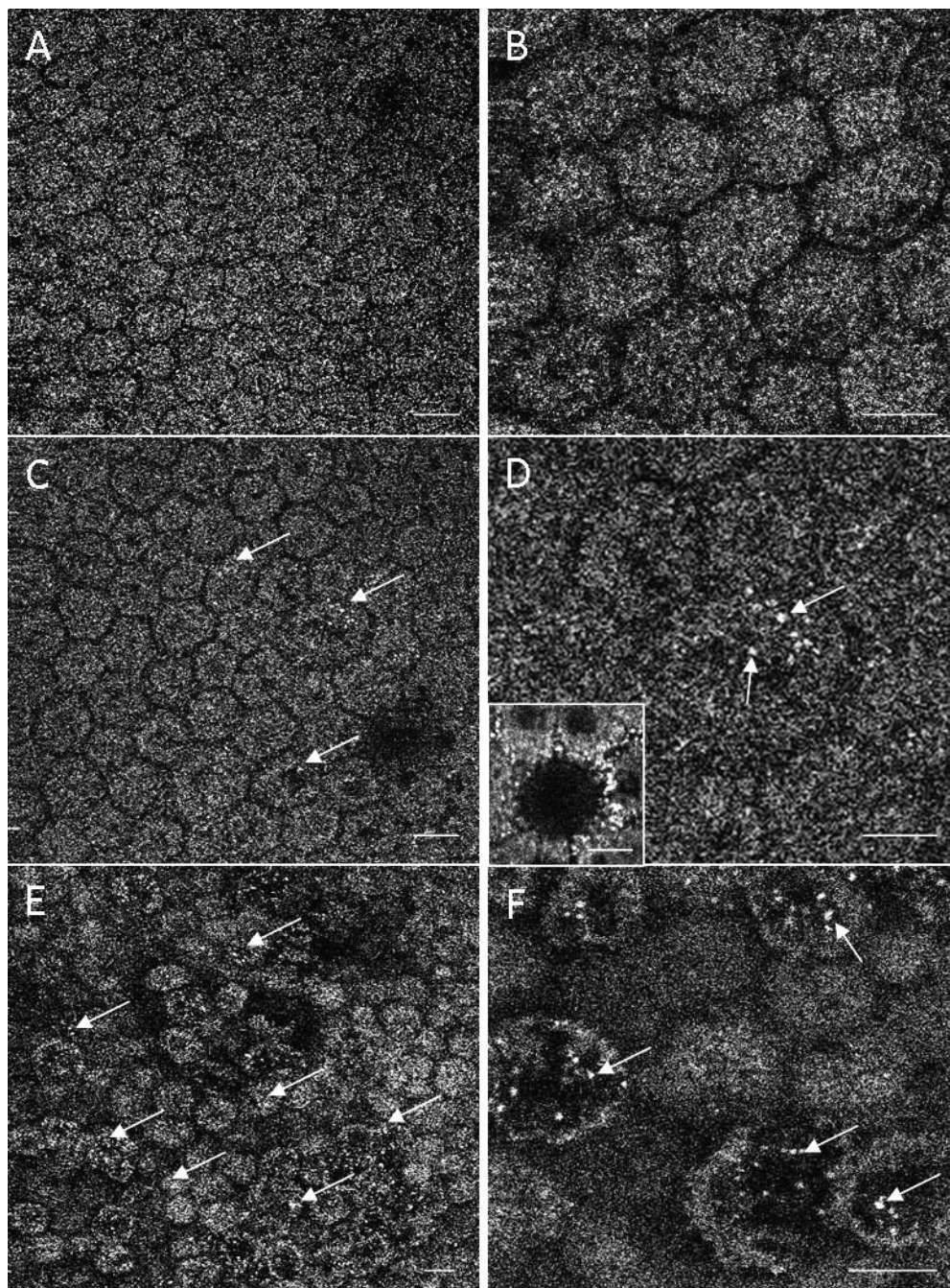


**FIGURE 7.** TPM-AF of the RPE exposed to different concentrations of  $\text{FeSO}_4$ . (A, B) 0 mM (no exposure). (C, D) 1 mM. (E, F) 10 mM of  $\text{FeSO}_4$  was added in the tissue culture medium and incubated for 1 hour. After that the medium was completely replaced by a normal medium and TPM-AF was examined.  $\text{FeSO}_4$  exposure induced the appearance of bright AF spots (arrows) inside and around RPE cells, as observed around laser photocoagulation spots.  $\lambda_{\text{ex}} = 750$  nm. Scale bar: 10  $\mu\text{m}$  (A-F).

the fluorescence intensity of the laser- or iron-induced bright AF shows milder decrease at the range of 740 to 790 nm excitation wavelengths and exhibits significantly higher fluorescence intensity than melanosome-AF in this range. As indicated from these results, the induced bright AF can be recognized the best around the excitation wavelength at 750 nm, where the difference of the intensities between the oxidative-damage induced AF and melanosome-AF is the largest. Therefore, the following experiments with TPM and FLIM were conducted with an excitation wavelength of 750 nm.

**Emission Spectrum.** Figure 8B shows the emission spectra of laser- or iron-induced AF spots and the melanosome-AF at the excitation wavelength 750 nm. The fluorescence intensities are normalized to the maximal value of the induced AF spots at 450 to 500 nm. Both the induced AF and the melanosome-AF have their emission peaks in channel 2 (450–500 nm), where the emission spectrum of induced AF spots shows significantly higher peak at 450 to 500 nm compared with the melanosome-AF.

**Fluorescence Lifetime.** Figure 9 presents the AF and FLIM images around the photocoagulation (Figs. 9A–F) and after

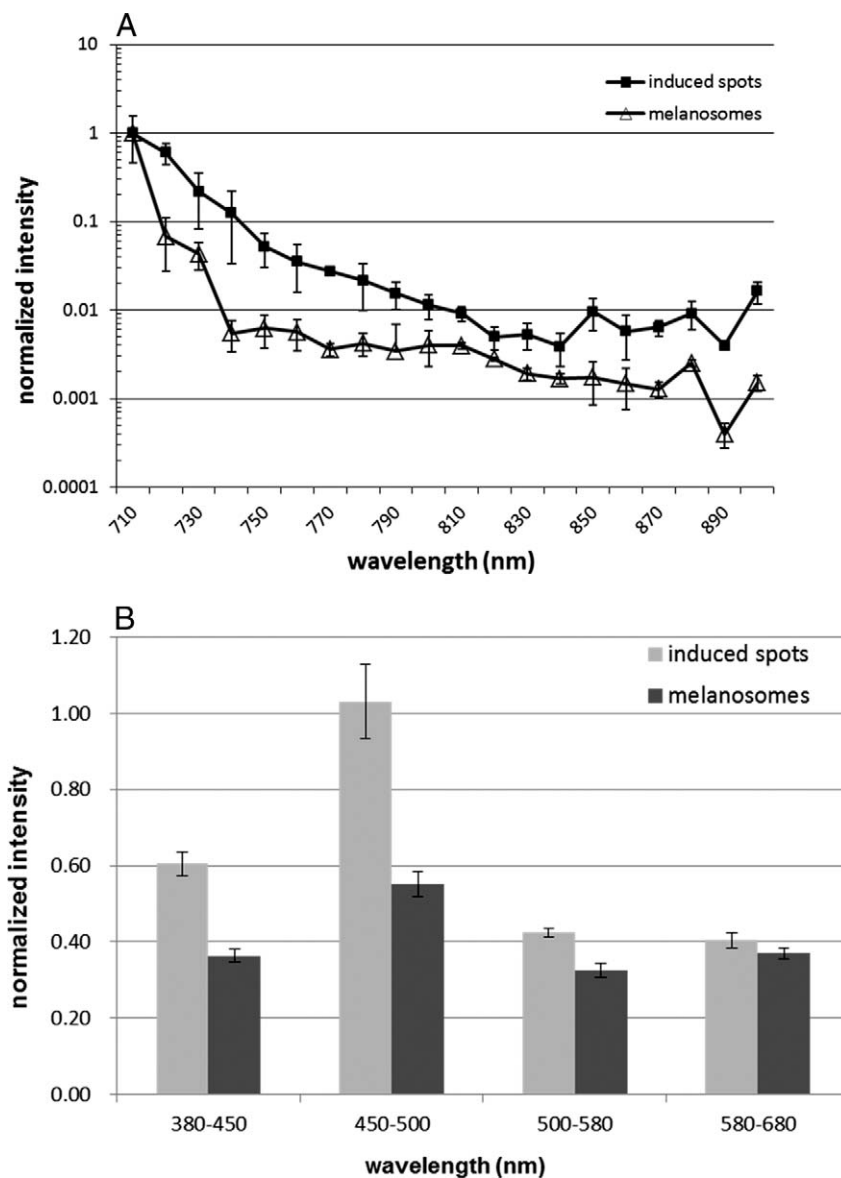


**FIGURE 8.** Excitation and emission spectrum of the melanosome-AF and the laser- or iron-induced bright AF. **(A)** Fluorescence intensity (emission range from 380–680 nm) at different excitation wavelengths. **(B)** Emission intensity analyzed with 4-channel analysis (channel 1: 380–450 nm; channel 2: 450–500 nm; channel 3: 500–580 nm; channel 4: 580–680 nm) at 750-nm excitation. **(A)** The fluorescence intensity of the bright AF spots induced by laser or iron is significantly stronger than the melanosome-AF in the excitation range of 740 nm to 790 nm. **(B)** The induced bright AF and melanosome-AF have their emission peaks in channel 2 (450–500 nm), whereas the relative fluorescence intensity in this range is significantly higher with the induced AF than the melanosome-AF.

FeSO<sub>4</sub> exposure (Figs. 9G–J). The color images are the pseudocolor presentations of FLT of the TPM-AF shown on their left. The blue color indicates short FLT, the orange color longer FLT. The bright granular AF induced by laser and iron have obviously longer FLT than of melanosome-AF. Figure 10 shows an exemplary FLIM image (Fig. 10A) and fluorescence decay curves (Figs. 10B, 10C). Figures 10B and 10C show the fluorescence decay curves of melanosome-AF and an iron-induced bright AF spot, respectively. The time and amplitude of each component as well as the mean FLT ( $t_m$ ) are presented in the tables below the decay curves. In the decay curve,  $x$ -axis indicates the time counted in the TCSPC method as a decay time of a photon (described in Materials and Methods section) and the  $y$ -axis indicates the number of the photons. The FLT

decay curve of melanosomes in RPE cell was fitted by a two-exponential decay curve (Fig. 10B) while the FLT decay curve of the laser- or iron-induced bright AF spots was fitted by three-exponential (Fig. 10C). The bright AF spot shown in Figure 10A (arrow) had a mean FLT ( $t_m$ ) of 2087 ps. The FLT components and mean time of more than 30 different laser- or iron-induced bright AF spots as well as of melanosomes were analyzed and the average data is shown in the Table. The average mean FLT of the melanosomes in RPE cell was  $117 \pm 19$  ps, while the FLT of induced bright AF spots was  $1388 \pm 700$  ps, which is significantly longer than the melanosome-FLT ( $P < 0.01$ ). There is no statistically significant difference between the FLT of laser-induced AF and iron-induced AF spots.

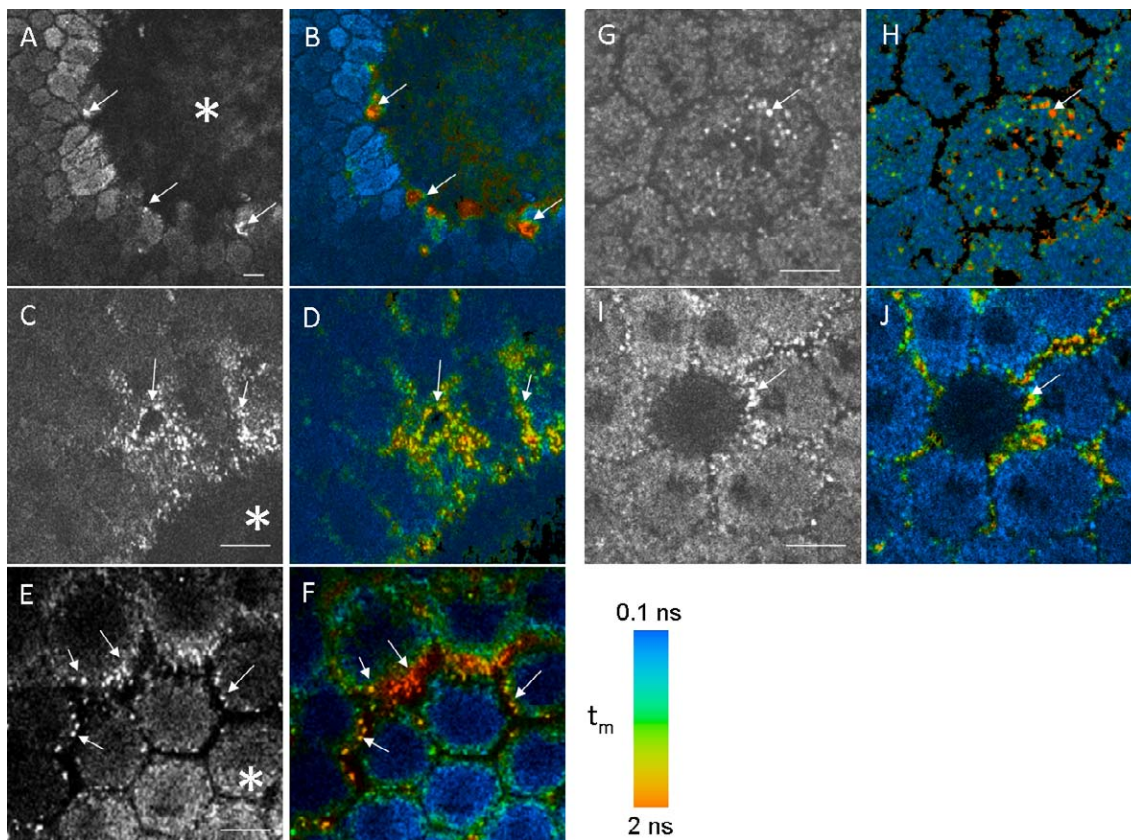


FIGURE 9. TPM and FLIM images of laser- or iron-induced RPE cells with the appearance of bright AF spots. (A-F) The RPE around photocoagulation. Asterisks (\*) indicate the lesion of the coagulation. (G-J) The RPE exposed to 1 mM FeSO<sub>4</sub> for 1 hour. Arrows indicate the bright AF induced by the stress. (A, C, E, G, D) TPM-AF ( $\lambda_{ex} = 750$  nm). (B, D, F, H, J) FLIM image ( $\lambda_{ex} = 750$  nm). FLIM image shows the FLT of the AF detected in each TPM image. FLT is presented with pseudocolor, where blue indicates a shorter FLT and the orange a longer FLT.  $t_m$ : mean FLT.

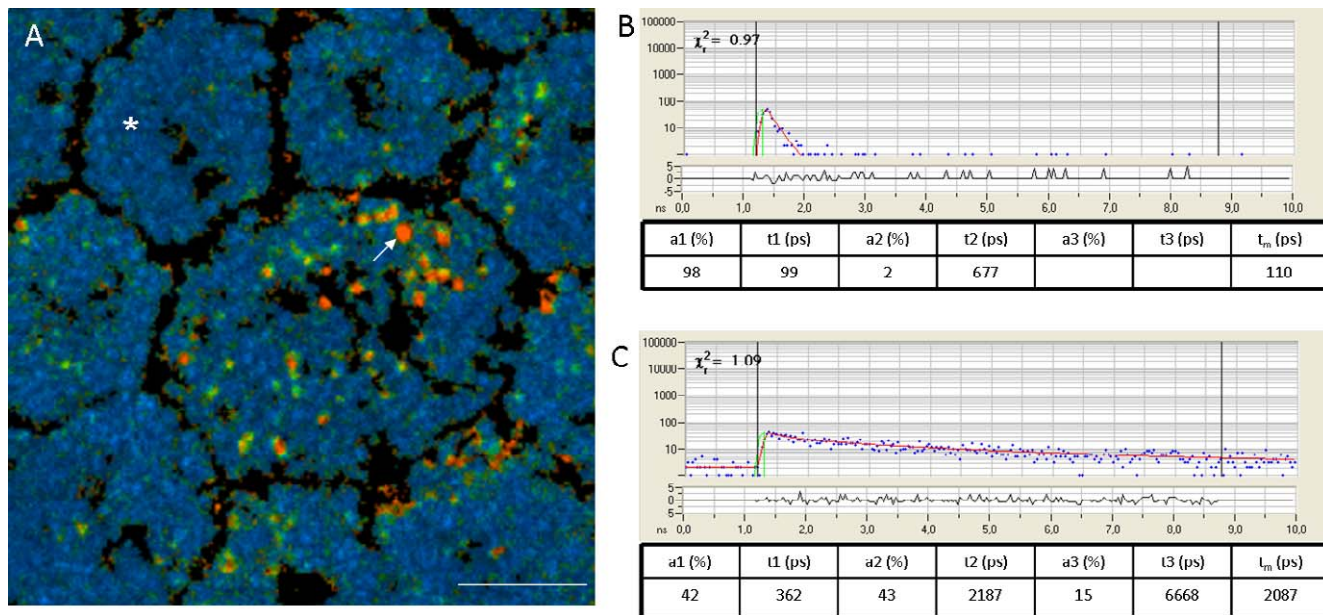


FIGURE 10. Comparison of fluorescence decay curves of melanosome-AF and iron-induced AF (A) FLIM image of the RPE exposed to 1 mM FeSO<sub>4</sub>, with the appearance of granular-formed AF with longer FLT (shown also in Fig. 9H). Scale bar: 10  $\mu$ m. (B, C) Decay curves obtained by time-correlated single photon counting of melanosome-AF (B) and the iron-induced AF (C). X-axis indicates the time and the y-axis indicates the number of the photons. Blue dot represents the number of the counted photons for the different lifetimes, and the red line is its best-fit exponential curve. The tables show the components of the exponential curve with amplitude (%) and time (ps). The mean FLT ( $t_m$ ) is calculated as shown in the Materials and Methods section. (B) The decay curve of the melanosomes (asterisk in [A]) fits to a two-exponential curve, which is composed mostly (98%) of the first shortest component (99 ps). The  $t_m$  calculated at this lesion was 110 ps. (C) The decay curve of the iron-induced AF indicated by arrow in (A) fits best to the curve with three-exponential components. The longest component (a3) is more than 6000 ps. The  $t_m$  for this AF was 2087 ps.

**TABLE.** Comparison of FLT Components and Mean FLT of the Melanosomes in RPE, Isolated Melanosomes, Isolated Melanosomes Under Oxidative Stress, and the Laser- or Iron-Induced Bright AF Spots

	Component Number	a1, %	t1, ps	a2, %	t2, ps	a3, %	t3, ps	t <sub>m</sub> ,* ps
Melanosomes in RPE, explant	2	94	93	6	533			117 ± 19
Isolated melanosomes	1	100	108					108 ± 15
Isolated melanosomes under oxidative stress	1	100	102					102 ± 12
Bright AF spots under oxidative stress	3	69	467	20	2620	11	5280	1388 ± 700

\* Mean ± standard deviation.

The data of FLT ( $\lambda_{\text{ex}} = 750 \text{ nm}$ ) from more than 30 different sample lesions were analyzed and the average values are shown in this table. The mean FLT ( $t_m$ ) of the melanosomes in RPE cell ( $117 \pm 19 \text{ ps}$ ) and isolated melanosomes ( $108 \pm 15 \text{ ps}$ ) are not significantly different, and there was no significant change under oxidative stress ( $102 \pm 12 \text{ ps}$ ). The average of  $t_m$  of the laser- or iron-induced bright AF spots was  $1388 \pm 700 \text{ ps}$ , whose decay fits the best as a three-exponential curve with the shortest component at  $467 \text{ ps}$  (69%) and the longest component longer than  $5000 \text{ ps}$  (11%).

## AF and FLIM of Isolated Melanosomes

In order to exclude the possibility, that the laser- or iron-induced bright AF signals are identical to the AF of oxidized melanosomes, isolated melanosomes were examined with TPM and FLIM under normal and oxidative stress conditions. The mean FLT of isolated melanosomes is  $108 \pm 15 \text{ ps}$ , which is not significantly different from the FLT of the melanosomes in RPE cell ( $117 \pm 19 \text{ ps}$ ). Oxidative stress did not change the FLT of melanosome-AF ( $102 \pm 12 \text{ ps}$ ; Table).

## DISCUSSION

Noninvasive and sensitive methods to detect cellular functional changes are desirable in basic research, as well as in clinical diagnostics. TPM and FLIM enable the detection of intracellular AF with high spatial resolution at low photochemical tissue damage. Detected AF signals cannot only be characterized by the excitation/emission spectrum, but by its three-dimensional morphology and with the fluorescence lifetime (FLT).

Spectral and time-resolved measurement of AF in different layers of the porcine ocular fundus with TPM was first presented by Peters et al.<sup>37</sup> Here we investigate two-photon excited AF together with FLT in living RPE cells, in which pathological changes of RPE-AF were experimentally induced and detected noninvasively using ex-vivo RPE. Melanosomes showed a high AF level and a short FLT, which is consistent with previous studies.<sup>38,39</sup> In the current study, we detected bright granular AF inside and around the RPE cells around thermal laser irradiation sites and following exposure to high dose of iron ion. FLIM revealed that the FLT of these oxidative damage-induced AF is significantly longer than the melanosome-AF.

The mechanisms of the formation of the oxidative stress-induced bright AF remain still unclear. Appearance of oxidative stress-induced lipofuscin-like fluorescence in RPE cells has been suggested previously.<sup>32,33,40,41</sup> In the studies of Katz et al., lipofuscin-like fluorescent pigments were induced in rat eyes by the intravitreal injection of ferrous sulfate.<sup>32,33,40</sup> Kayatz et al. presented that strong oxidation by hydrogen peroxide might induce melanin fluorescence in the RPE observed with fluorescence microscopy and suggested that the oxidation of melanosomes is involved in lipofuscin formation.<sup>41</sup> However, most of these studies did not characterize these AF molecules in more detail.

TPM on mouse RPE was previously reported by Imanishi et al.<sup>42,43</sup> They imaged mouse RPE in vivo through the sclera and showed the structure of retinyl ester storage around RPE cells, which is excited at  $730 \text{ nm}$ . Compared with their study, in our current study the TPM-AF image of the porcine RPE appears quite different, in which melanosome-AF is the most intensive, and the typical AF granules located around RPE cells as shown

in their study are not detectable under normal conditions. However, interestingly, the similar AF granular spots around RPE cell are detectable once the RPE is strongly oxidized in our model. The reasons are considered as following: the mice in the study of Imanishi et al.<sup>42</sup> were albino mice and, therefore, they did not have any strong melanosome-AF as seen in our study. In porcine RPE cells, similar to human RPE cells, a large number of melanosomes exist inside of the cell and the melanosome-AF is dominant in TPM under physiological conditions. However, under oxidative stress, the formation of strongly fluorescent molecules might be induced, so that their AF is clearly detected. Although the bright AF spots around RPE cells in our study may also originate from oxidized retinyl ester storage as Imanishi et al.<sup>42</sup> suggested, the strong AF induced by oxidative stress appears not only around the cell, but also inside the cell. Therefore, the localization of oxidative stress-induced AF granules does not correspond completely to the retinyl ester storage around the cells that they presented. Another possibility is that the AF derives from oxidized melanosomes or other cellular basic organelles and phagocytized photoreceptor outer segments. Among these, we could exclude in this study the possibility of the oxidized melanosomes. FLIM results clearly suggest that the AF of oxidized melanosomes has similar FLT to the melanosome-AF under normal conditions. Since to date the fluorescence properties of most RPE components have not been investigated with TPM or FLIM, further thorough investigations are required in order to elucidate the origin and formation mechanisms of the oxidative-damage induced bright AFs in RPE cells.

In contrast to the melanosome-FLT, the bright AF spots induced by laser or iron ion show a varying FLT, from approximately  $600 \text{ ps}$  to  $2000 \text{ ps}$  with a mean lifetime of  $1388 \text{ ps}$ . There was no statistical difference between laser- and iron-induced AF regarding their FLT, indicating that these different methods induce similar functional oxidative changes in RPE cells. We assume that this wide range of FLT is due to the extent of the molecular changes induced by oxidative stress such as alteration of protein binding. Finding the responsible molecules for this FLT change is required for further understanding.

Measured FLT may vary to some extent among the instruments and measurement setups, especially in the range of very short FLT. Compared with the study by Peters et al., where the FLT of the RPE-melanosomes was reported to be approximately  $70 \text{ ps}$ ,<sup>37</sup> the average melanosome-FLT measured in the current study was longer ( $t_m = 117 \text{ ps}$ ). This difference might be caused by the longer instrumental response function in FLT measurement and a longer lifetime component which is caused by an additional fluorescence component. Due to the instrumental response function of our FLIM setup, it was not able to resolve lifetime components shorter than  $90 \text{ ps}$ . Although this kind of difference among the instruments or parameters setups is still unavoidable, it is significantly

meaningful to investigate the relative alteration of FLT for the functional monitoring of RPE cell.

The RPE cells we used in the current study are from relatively young porcine eyes, which contain very few lipofuscin. Although RPE with few lipofuscin might not be the ideal model to study age-related cellular changes, the young porcine RPE might be useful to investigate the cellular responses to pathological conditions or the formation of lipofuscin-like fluorescent molecules in RPE cells, as steps in the lipofuscinogenesis.

According to the previous studies, two-photon excited lipofuscin-AF has a maximal excitation around at 800 nm with peak fluorescence around 500 to 550 nm,<sup>44-46</sup> while in one-photon excitation the fluorescence spectrum of lipofuscin or its main fluorescence component A2E is  $\lambda_{ex}/\lambda_{em} \approx 400$  to 500/550 to 650 nm.<sup>47-49</sup> The bright granular AF induced by oxidative stresses in the current study were excited the most at 710 to 750 nm and emission peak was in the range of 450 to 500 nm, which is different from the characteristics of lipofuscin-AF examined in previous studies with TPM. However, the previous study with human lipofuscin was performed under 4% paraformaldehyde fixation and mounting,<sup>44,46</sup> which can alter the natural fluorescence properties. As there is no other study performed with human lipofuscin concerning TPM-AF, to compare the fluorescence properties of induced AF in our results, measurement of human lipofuscin with TPM under living condition (in vivo or ex vivo) is required.

There are a few previous reports measuring the FLT of lipofuscin and A2E, one of the major fluorescent components of lipofuscin.<sup>49,50</sup> In the study of Schweitzer et al., lipofuscin-FLT (one-photon excitation,  $\lambda_{ex} = 446$  nm) was shown with biexponential approximation,  $t_1 = 390$  ps (48%) and  $t_2 = 2240$  ps (52%), whereas A2E-FLT was shown much shorter,  $t_1 = 170$  ps (98%) and  $t_2 = 1120$  (2%).<sup>50</sup> The FLT of the induced bright AF in the current study seems to be relatively closer to their lipofuscin-FLT than to the A2E-FLT, but not identical. It is required to elucidate FLT of other fluorescent component of lipofuscin. Considering from the results of the current and previous studies of fluorescence spectrum and FLIM, the oxidative stress-induced bright AF in RPE cell might be composed partially of similar substances of lipofuscin, but they are not identical. Further investigation is certainly necessary to identify the origin of oxidative stress-induced granular bright AF.

FLIM is a new technology which is widely used in many scientific fields, and is also in ophthalmology greatly expected to realize functional imaging of the fundus.<sup>50-53</sup> Schweitzer et al. reported time-resolved AF imaging of human retina with FLIM ophthalmoscopy, which they introduced recently for a clinical use.<sup>50-52</sup> They recently reported a thorough study on the FLT of subretinal drusens of donor eyes.<sup>53</sup> The current problem is, however, there is still too little basic knowledge concerning AF and FLIM in fundus tissues and RPE cells for interpretation of in vivo FLIM images. Therefore, it is of great importance to investigate time-resolved AF of RPE or photoreceptors at the cell level for the right interpretation of in vivo FLIM images. The use of fundus FLIM ophthalmoscopy based on sufficient basic data is required and it might provide a great possibility to detect early functional damages of RPE cell in patients that are not detectable to date. Since RPE functional decline is significantly related to the pathogenesis of various chorioretinal disorders, such as AMD, fundus FLIM might be a useful tool for the early diagnosis of these disorders, as well as therapy control or prognostic expectation.

In summary, a recently induced technology for live-cell imaging, AF-TPM combined with FLIM could elucidate RPE cell functional changes noninvasively using ex vivo tissue. In the current study, TPM could detect oxidative stress-induced bright

AF appearance inside and around RPE cells. FLIM could reveal that these induced AF granules have significantly longer FLT than the melanosomes. Results obtained in the current study would provide useful insights for interpretation of fundus AF and FLIM ophthalmoscopy in clinical practice. Moreover, studies on the formation mechanisms of oxidative stress induced-bright AF granules will provide further understanding about lipofuscinogenesis and related cellular functional alterations of RPE cells. In order to elucidate more details about pathological changes of AF and FLIM of RPE and their surrounding tissues, further investigation is now being conducted.

### Acknowledgments

The authors thank Astrid Rodewald and Barbara Flucke for their technical assistance.

Supported by German Federal Ministry of Education and Research (BMBF) Grant 01EZ0733.

Disclosure: **Y. Miura**, None; **G. Huettmann**, None; **R. Orzekowsky-Schroeder**, None; **P. Steven**, None; **M. Szaszák**, None; **N. Koop**, None; **R. Brinkmann**, None

### References

- Schenke-Layland K, Riemann I, Damour O, Stock UA, König K. Two-photon microscopes and in vivo multiphoton tomographs—powerful diagnostic tools for tissue engineering and drug delivery. *Adv Drug Deliv Rev.* 2006;58:878-896.
- Rubart M. Two-photon microscopy of cells and tissue. *Circ Res.* 2004;95:1154-1166.
- Steven P, Müller M, Koop M, Rose C, Hüttmann G. Comparison of confocal and two-photon microscopy for non-invasive imaging of ocular surface pathologies. *J Biomed Opt.* 2009;14:064040.
- Gehlsen U, Hüttmann G, Steven P. Intravital multidimensional real-time imaging of the conjunctival immune system. *Dev Ophthalmol.* 2010;45:40-48.
- Crosignani V, Dvornikov A, Aguilar JS, et al. Deep tissue fluorescence imaging and in vivo biological applications. *J Biomed Opt.* 2012;17:116023.
- Cahalan MD, Parker I, Wei SH, Miller MJ. Two-photon tissue imaging: seeing the immune system in a fresh light. *Nav Rev Immunol.* 2002;2:872-880.
- Mayevsky A, Rogatsky GG. Mitochondrial function in vivo evaluated by NADH fluorescence: from animal models to human studies. *Am J Physiol Cell Physiol.* 2007;292:C615-C640.
- Thorell B. Flow-cytometric monitoring of intracellular flavins simultaneously with NAD(P)H levels. *Cytometry.* 1983;4:61-65.
- Kiefer CR, McKenney JB, Trainor JF, et al. Porphyrin loading of lipofuscin granules in inflamed striated muscle. *Am J Pathol.* 1998;153:703-708.
- Eldred GE, Miller GV, Stark WS, Feeney-Burns L. Lipofuscin: resolution of discrepant fluorescence data. *Science.* 1982;216:757-759.
- Gareau DS, Bargo PR, Horton WA, Jacques SL. Confocal fluorescence spectroscopy of subcutaneous cartilage expressing green fluorescent protein versus cutaneous collagen autofluorescence. *J Biomed Opt.* 2004;9:254-258.
- König K, Schenke-Layland K, Riemann I, Stock UA. Multiphoton autofluorescence imaging of intratissue elastic fibers. *Biomaterials.* 2005;26:495-500.
- Solbach U, Keilhauer C, Knabben H, Wolf S. Imaging of retinal autofluorescence in patients with age-related macular degeneration. *Retina.* 1997;17:385-389.

14. Delori FC, Dorey CK, Staurengi G, Arend O, Goger DG, Weiter JJ. In vivo fluorescence of the ocular fundus exhibits retinal pigment epithelium lipofuscin characteristics. *Invest Ophthalmol Vis Sci.* 1995;36:718-729.
15. Matsumoto H, Kishi S, Sato T, Mukai R. Fundus autofluorescence of elongated photoreceptor outer segments in central serous chorioretinopathy. *Am J Ophthalmol.* 2011;151:617-623.e1.
16. Sekiryu T, Iida T, Maruko I, Saito K, Kondo T. Infrared fundus autofluorescence and central serous chorioretinopathy. *Invest Ophthalmol Vis Sci.* 2010;51:4956-4962.
17. Kellner U, Kellner S, Weintz S. Fundus autofluorescence (488 NM) and near-infrared autofluorescence (787 NM) visualize different retinal pigment epithelium alterations in patients with age-related macular degeneration. *Retina.* 2010;30:6-15.
18. Peng XJ, Zhang WF. Lipofuscin- and melanin-related fundus autofluorescence in patients with submacular idiopathic choroidal neovascularization. *Yan Ke Xue Bao.* 2012;27:138-142.
19. Lakowicz JR, Szmajdzinski H, Nowaczyk K, Johnson ML. Fluorescence lifetime imaging of free and protein-bound NADH. *Proc Natl Acad Sci U S A.* 1992;89:1271-1275.
20. Tanaka F, Tamai N, Yamazaki I, Nakashima N, Yoshihara K. Temperature-induced changes in the coenzyme environment of D-amino acid oxidase revealed by the multiple decays of FAD fluorescence. *Biophys J.* 1989;56:901-909.
21. Szaszak M, Steven P, Shima K, et al. Fluorescence lifetime imaging unravels C. trachomatis metabolism and its crosstalk with the host cell. *PLoS Pathog.* 2011;7:e1002108.
22. Gehlsen U, Oetke A, Szaszak M, et al. Two-photon fluorescence lifetime imaging monitors metabolic changes during wound healing of corneal epithelial cells in vitro. *Graefes Arch Clin Exp Ophthalmol.* 2012;250:1293-1302.
23. Christen WG, Glynn RJ, Hennekens CH. Antioxidants and age-related eye disease. Current and future perspectives. *Ann Epidemiol.* 1996;6:60-66.
24. Cai J, Nelson KC, Wu M, Sternberg P Jr, Jones DP. Oxidative damage and protection of the RPE. *Prog Retin Eye Res.* 2000;19:205-221.
25. Chowers I, Wong R, Dentchev T, et al. The iron carrier transferrin is upregulated in retinas from patients with age-related macular degeneration. *Invest Ophthalmol Vis Sci.* 2006;47:2135-2140.
26. Dunaief JL. Iron induced oxidative damage as a potential factor in age-related macular degeneration: the Cogan Lecture. *Invest Ophthalmol Vis Sci.* 2006;47:4660-4664.
27. Cleary CA, Jungkim S, Ravikumar K, Kelliher C, Acheson RW, Hickey-Dwyer M. Intravitreal bevacizumab in the treatment of neovascular age-related macular degeneration, 6- and 9-month results. *Eye (Lond).* 2008;22:82-86.
28. Muether PS, Hermann MM, Viebahn U, Kirchhof B, Fauser S. Vascular endothelial growth factor in patients with exudative age-related macular degeneration treated with ranibizumab. *Ophthalmology.* 2012;119:2082-2086.
29. Miura Y, Klettner A, Noelle B, Hasselbach H, Roeder J. Change of morphological and functional characteristics of retinal pigment epithelium cells during cultivation of retinal pigment epithelium-choroid perfusion tissue culture. *Ophthalmic Res.* 2010;43:122-133.
30. Orzekowsky-Schroeder R, Klinger A, Martensen B, et al. In vivo spectral imaging of different cell types in the small intestine by two-photon excited autofluorescence. *J Biomed Opt.* 2011;16:116025.
31. Becker W. Fluorescence lifetime imaging-techniques and applications. *J Microsc.* 2012;247:119-136.
32. Katz ML, Stientjes HJ, Gao CL, Christianson JS. Iron-induced accumulation of lipofuscin-like fluorescent pigment in the retinal pigment epithelium. *Invest Ophthalmol Vis Sci.* 1993;34:3161-3171.
33. Katz ML, Christianson JS, Gao CL, Handelman GJ. Iron-induced fluorescence in the retina: dependence on vitamin A. *Invest Ophthalmol Vis Sci.* 1994;35:3613-3624.
34. Terrasa A, Guajardo M, Catala A. Lipoperoxidation of rod outer segments of bovine retina is inhibited by soluble binding proteins for fatty acids. *Mol Cell Biochem.* 1998;178:181-186.
35. Fagali N, Catala A. Fe<sup>2+</sup> and Fe<sup>3+</sup> initiated peroxidation of sonicated and non-sonicated liposomes made of retinal lipids in different aqueous media. *Cbem Phys Lipids.* 2009;159:88-94.
36. Boulton M, Marshall J. Repigmentation of human retinal pigment epithelial cells in vitro. *Exp Eye Res.* 1985;41:209-218.
37. Peters S, Hammer M, Schweitzer D. Two-photon excited fluorescence microscopy application for ex vivo investigation of ocular fundus samples. *Proc SPIE.* 2011;8086:808605.
38. Teuchner K, Freyer W, Leupold D, et al. Femtosecond two-photon excited fluorescence of melanin. *Photochem Photobiol.* 1999;70:146-151.
39. Dimitrow E, Riemann I, Ehlers A, et al. Spectral fluorescence lifetime detection and selective melanin imaging by multiphoton laser tomography for melanoma diagnosis. *Exp Dermatol.* 2009;18:509-515.
40. Katz ML, Shanker MJ. Development of lipofuscin-like fluorescence in the retinal pigment epithelium in response to protease inhibitor treatment. *Mech Ageing Dev.* 1989;49:23-40.
41. Kayatz P, Thumann G, Luther TT, et al. Oxidation causes melanin fluorescence. *Invest Ophthalmol Vis Sci.* 2001;42:241-246.
42. Imanishi Y, Batten ML, Piston DW, Baehr W, Palczewski K. Noninvasive two-photon imaging reveals retinyl ester storage structures in the eye. *J Cell Biol.* 2004;164:373-383.
43. Palczewska G, Maeda T, Imanishi Y, et al. Noninvasive multiphoton fluorescence microscopy resolves retinal and retinal condensation products in mouse eyes. *Nat Med.* 2010;16:1444-1449.
44. Han M, Bindewald-Wittich A, Holz FG, et al. Two-photon excited autofluorescence imaging of human retinal pigment epithelial cells. *J Biomed Opt.* 2006;11:010501.
45. Eichhoff G, Busche MA, Garaschuk O. In vivo calcium imaging of the aging and diseased brain. *Eur J Nucl Med Mol Imaging.* 2008;35(suppl 1):S99-S106.
46. Bindewald-Wittich A, Han M, Schmitz-Valckenberg S, et al. Two-photon-excited fluorescence imaging of human RPE cells with a femtosecond Ti: Sapphire laser. *Invest Ophthalmol Vis Sci.* 2006;47:4553-4557.
47. Lamb LE, Simon JD. A2E: a component of ocular lipofuscin. *Photochem Photobiol.* 2004;79:127-136.
48. Framme C, Schule G, Birngruber R, et al. Temperature dependent fluorescence of A2-E, the main fluorescent lipofuscin component in the RPE. *Curr Eye Res.* 2004;29:287-291.
49. Cubeddu R, Taroni P, Hu DN, Sakai N, Nakanishi K, Roberts JE. Photophysical studies of A2-E, putative precursor of lipofuscin, in human retinal pigment epithelial cells. *Photochem Photobiol.* 1999;70:172-175.
50. Schweitzer D, Schenke S, Hammer M, et al. Towards metabolic mapping of the human retina. *Microsc Res Tech.* 2007;70:410-419.
51. Schweitzer D, Hammer M, Schweitzer F, et al. In vivo measurement of time-resolved autofluorescence at the human fundus. *J Biomed Opt.* 2004;9:1214-1222.
52. Schweitzer D, Quick S, Schenke S, et al. Comparison of parameters of time-resolved autofluorescence between healthy subjects and patients suffering from early AMD. *Ophthalmology.* 2009;106:714-722.
53. Schweitzer D, Gaillard ER, Dillon J, et al. Time-resolved autofluorescence imaging of human donor retina tissue from donors with significant extramacular drusen. *Invest Ophthalmol Vis Sci.* 2012;53:3376-3386.